

## Counterflow of Electrons in Two Isolated Quantum Point Contacts

V. S. Khrapai,<sup>1,2</sup> S. Ludwig,<sup>1</sup> J. P. Kotthaus,<sup>1</sup> H. P. Tranitz,<sup>3</sup> and W. Wegscheider<sup>3</sup>

<sup>1</sup>Center for NanoScience and Department für Physik, Ludwig-Maximilians-Universität, Geschwister-Scholl-Platz 1, D-80539 München, Germany

<sup>2</sup>Institute of Solid State Physics RAS, Chernogolovka, 142432, Russian Federation

<sup>3</sup>Institut für Experimentelle und Angewandte Physik, Universität Regensburg, D-93040 Regensburg, Germany

(Received 2 April 2007; published 31 August 2007)

We study the interaction between two adjacent but electrically isolated quantum point contacts (QPCs). At high enough source-drain bias on one QPC, the drive QPC, we detect a finite electric current in the second, unbiased, detector QPC. The current generated at the detector QPC always flows in the opposite direction than the current of the drive QPC. The generated current is maximal, if the detector QPC is tuned to a transition region between its quantized conductance plateaus and the drive QPC is almost pinched-off. We interpret this counterflow phenomenon in terms of an asymmetric phonon-induced excitation of electrons in the leads of the detector QPC.

DOI: 10.1103/PhysRevLett.99.096803

PACS numbers: 73.23.Ad, 73.50.Lw, 73.63.Rt

The state of a confined quantum system is modified by interactions with an external field (or with external sources of energy). In semiconductor nanostructures the energy and quasimomentum of electrons acting as probe are strongly influenced by the environment, e.g., via electron-electron or electron-phonon interaction. If driven out of equilibrium, Coulomb forces establish the local equilibrium within the electron system whereas electron-phonon interactions dominate the energy exchange with the environment [1]. Drag experiments in semiconductor nanostructures provide a tool to study the effect of external electrons or phonons onto a probe electron system.

Current drag between parallel two-dimensional (2D) electron layers has been investigated in GaAs/AlGaAs bilayer systems. At small interlayer separations, observations are consistent with the Coulomb drag phenomenon [2]. At larger separations virtual-phonon exchange has been invoked to explain the data [3]. A negative sign of a current drag between 2D and 3D electron gases in GaAs was explained by the Peltier effect [4]. At high filling factors in a perpendicular magnetic field a sign change of the longitudinal drag between parallel 2D layers was found as a function of the imbalance of the electron density in the two layers [5,6].

Interactions between two lateral quantum wires in GaAs have been investigated in Ref. [7]. The observed frictional drag, strongly oscillating as a function of the one-dimensional (1D) subband occupation, was interpreted in terms of Coulomb interaction between two Luttinger liquids. Recently, the observation of negative Coulomb drag between two disordered lateral 1D wires in GaAs in perpendicular magnetic fields was reported [8].

Here we report on a novel interaction effect between two neighboring quantum point contacts (QPCs), embedded in mutually isolated electric circuits. When a strong current is flowing through the partially transmitting drive QPC, we detect a small current in the second, unbiased, detector QPC. The detector current flows in the

opposite direction of the drive current and shows a non-linear dependence on the source-drain bias of the drive QPC. It oscillates as a function of the detector QPC transmission. We suggest an explanation of this counterflow effect in terms of asymmetric phonon-induced excitation of ballistic electrons in the leads of the detector QPC.

Our samples are prepared on a GaAs/AlGaAs heterostructure containing a two-dimensional electron gas 90 nm below the surface, with an electron density of  $n_S = 2.8 \times 10^{11} \text{ cm}^{-2}$  and a low-temperature mobility of  $\mu = 1.4 \times 10^6 \text{ cm}^2/\text{Vs}$ . An atomic force microscope (AFM) micrograph of the split-gate nanostructure, produced with *e*-beam lithography, is shown in the left inset of Fig. 1. The negatively biased central gate *C* divides the electron system into two separate circuits, and prevents leakage currents between them. Two QPCs are defined on the upper and lower side of the gate *C*, respectively, by biasing gates 8 and 3. Other gates are grounded if not mentioned.

The right inset of Fig. 1 shows a sketch of the counterflow experiment. We use separate electric circuits for the (upper) drive QPC and (lower) detector QPC. A dc bias voltage,  $V_{\text{drive}}$ , is applied to the left lead of the drive QPC, while the right lead is grounded. A current-voltage amplifier with an input voltage offset of about  $10 \mu\text{V}$  is connected to the right lead of the detector QPC. Its left lead is always maintained at the same offset potential in order to assure zero voltage drop across the detector QPC. In both circuits, a positive sign of the current corresponds to electrons flowing to the left. For differential counterflow conductance measurements, the drive bias is modulated at a frequency of 21 Hz and the resulting ac current component in the detector circuit is measured with lock-in detection in the linear response regime. All measurements are performed in a dilution refrigerator at an electron temperature below 150 mK. The experimental results are the same if detector and drive QPC are interchanged.

First, we characterize the QPCs using a standard differential conductance measurement. Figure 1 displays the

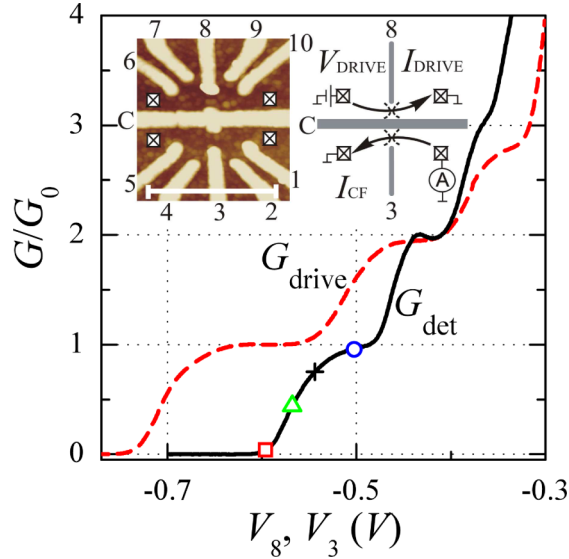


FIG. 1 (color online). Conductance of the drive QPC (dashed line) and the detector QPC (solid line) in the linear response regime as a function of respective gate voltages  $V_8$  and  $V_3$ . Symbols on the detector QPC curve mark the  $V_3$  values used for counterflow conductance measurement presented in Fig. 2(b). Left inset: AFM micrograph of the metal gates on the surface of the heterostructure (bright tone). Crossed squares mark contacted 2D electron gas regions. The scale bar equals  $1 \mu\text{m}$ . Right inset: sketch of the counterflow measurement. The directions of currents are shown for the case of  $V_{\text{drive}} > 0$ .

differential conductances of both QPCs in linear response, measured as a function of the respective gate voltage  $V_3$ , or  $V_8$ . At low gate voltages, the QPCs are pinched-off and the conductance is close to zero. With increasing gate voltage, 1D channels successively open up [9]. For both QPCs we observe three conductance plateaus approximately quantized in units of  $G_0 = 2e^2/h$ . With high bias spectroscopy [10] we find the spacing between the two lowest subbands to be approximately 4 meV (3 meV) for the drive (detector) QPC. The half-width of the energy window for opening a 1D subband is  $\Delta \approx 0.5$  meV in both QPCs.

Having characterized the QPCs, we turn to counterflow measurements. Figure 2(a) shows the dc counterflow current,  $I_{\text{cf}}$ , through the detector QPC and the differential counterflow conductance,  $g_{\text{cf}} \equiv dI_{\text{cf}}/dV_{\text{drive}}$ , as a function of the bias on the drive QPC. Here, the drive QPC is tuned to nearly half a conductance quantum  $G_{\text{drive}} = G_0/2$ , while the detector QPC is in the pinch-off regime (i.e., the lowest 1D subband bottom is well above the Fermi level) with  $G_{\text{det}} \approx 10 \text{ G}\Omega^{-1}$ . Surprisingly, for  $|V_{\text{drive}}| \geq 1$  mV, a finite current is observed in the unbiased detector circuit. The direction of  $I_{\text{cf}}$  is opposite to that of the drive QPC current  $I_{\text{drive}}$ . The dc counterflow current is a thresholdlike, nearly odd function of  $V_{\text{drive}}$ . Correspondingly, the differential counterflow conductance is negative and a nearly even function of  $V_{\text{drive}}$ . The sign of  $g_{\text{cf}}$  expresses a phase shift of  $\pi$  between the applied ac modulation of  $V_{\text{drive}}$  and the detected ac component of  $I_{\text{cf}}$ .

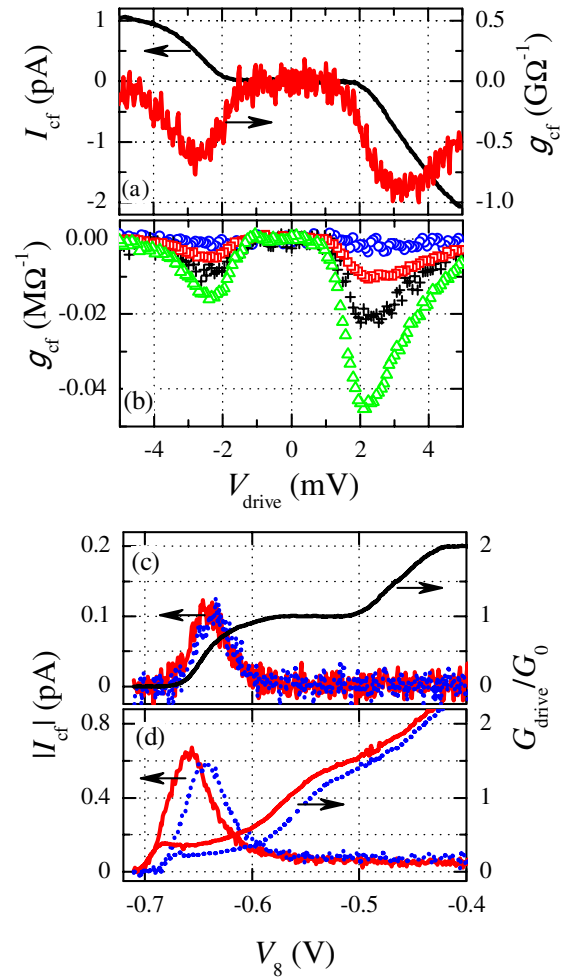


FIG. 2 (color online). (a)  $I_{\text{cf}}$  and  $g_{\text{cf}}$  for the nearly pinched-off detector QPC as a function of  $V_{\text{drive}}$ . (b)  $g_{\text{cf}}$  measured for a set of  $G_{\text{det}}$  values marked by according symbols in Fig. 1. (c),(d) Absolute value of  $I_{\text{cf}}$  as a function of the drive QPC gate voltage  $V_8$ , for  $V_{\text{drive}} = \pm 2.25$  mV (c) and  $V_{\text{drive}} = \pm 4$  mV (d). Also shown is the drive QPC's conductance in linear response (c) and its differential conductance at  $V_{\text{drive}} = \pm 4$  mV (d). Solid (dotted) lines correspond to  $V_{\text{drive}} < 0$  ( $> 0$ ). In (a),(b) gates 7 and 9 are grounded, while in (c),(d)  $V_7 = V_9 = -0.4$  V. The drive bias modulation used to measure  $g_{\text{cf}}$  is  $92 \mu\text{V}$  rms.

Figures 2(c) and 2(d) show the absolute value of  $I_{\text{cf}}$  for the nearly pinched-off detector as a function of the voltage on gate 8, which tunes the drive QPC transmission. The corresponding drive QPC differential conductance curves are also shown. For not too high  $V_{\text{drive}}$  [Fig. 2(c)], a non-zero counterflow current is only detected in the region between pinch-off and the first conductance plateau of the drive QPC. For higher  $V_{\text{drive}}$  [Fig. 2(d)]  $I_{\text{cf}}$  increases superlinearly with  $V_{\text{drive}}$  at its maximum and remains finite at higher gate voltages  $V_8$ . Since the source bias effects the potential distribution near the constriction, the nonlinear  $1/2$  conductance plateau of the drive QPC shifts when changing  $V_{\text{drive}}$  [10,11]. This causes the shift of the extrema

on Fig. 2(d) as well as the asymmetry of  $g_{cf}$  in Fig. 2(a) when reversing the bias.

We proceed to study the counterflow effect in the regime of a more opened detector QPC. Figure 2(b) plots  $g_{cf}$  [12] as a function of  $V_{drive}$  for several values of  $G_{det}$  between 0 and  $G_0$  (marked with the same symbols in Fig. 1). The qualitative appearance of  $g_{cf}(V_{drive})$  is independent of  $G_{det}$ . However, the amplitude of  $g_{cf}$  is a strongly nonmonotonic function of the detector transmission. The counterflow conductance reaches its maximum for  $G_{det} \approx G_0/2$  and decreases rapidly with further increasing  $G_{det}$ . Note that the absolute value of  $g_{cf}$  is small, corresponding to a maximal currents ratio of  $|I_{cf}/I_{drive}| \lesssim 10^{-3}$ .

In Fig. 3(a)  $g_{cf}$  is plotted as a function of  $V_3$ , controlling the detector transmission.  $V_{drive}$  and  $V_8$  are adjusted for maximal  $g_{cf}$  and kept fixed. Confirming the trend seen in Fig. 2(b), the measured  $g_{cf}$  (solid symbols) strongly oscillates with increasing  $V_3$  and displays three pronounced maxima before the detector QPC is fully opened. The position of the  $n$ th maximum ( $n = 0, 1, 2$ ) is close to the value of  $V_3$ , where  $G_{det}/G_0 \approx n + 0.5$  (Fig. 1). Here, the energy  $E_S^n$  of the bottom of the  $n$ th 1D subband of the detector QPC aligns with the Fermi level of the leads  $E_S^n \approx E_F$ . In contrast,  $g_{cf}$  is close to zero for fully transmitting 1D channels ( $G_{det}/G_0 \approx n + 1$ ). The overall magnitude of  $g_{cf}$  decreases with increasing  $V_3$ , hence  $G_{det}$ . This is caused by a finite series resistance  $R_{ext}$  of the external circuit, which results in a measured  $g_{cf}$  lower than the case for an ideal ammeter [13]. The corrected counterflow conductance,  $g_{cf}^{ideal} \equiv g_{cf}(1 + R_{ext}G_{det})$ , corresponding to  $R_{ext} = 0$ , is shown in Fig. 3(a) with open symbols. The corrected maxima are roughly equal in size and symmetric. Moreover, the shape of the  $n$ th maximum compares quite well with the corresponding function of the equilibrium transmission  $T_n(1 - T_n)$ , extracted from the conductance data  $T_n \equiv G_{det}/G_0 - n$  [dashed lines in Fig. 3(a)].

In Fig. 3(b) we plot the normalized  $g_{cf}$  and the transmission function  $4T_0(1 - T_0)$  on a logarithmic scale near the detector pinch-off. In the pinch-off regime (i.e., for  $T_0 \ll 1$ ) the transmission probability of a QPC is expressed as  $T_0(E) \propto \exp([E - E_S^0]/\Delta)$  [11]. Here  $E$  is the kinetic energy of current carrying electrons and  $\Delta$  is the half-width of the energy window for opening a 1D subband. The energy  $E_S^0$  of the detector QPC is controlled by gate 3 via  $E_S^0 \propto -|e|V_3$ . This explains a nearly exponential drop of the transmission function with decreasing  $V_3$  [Fig. 3(b)]. In contrast, the measured  $g_{cf}$  drops considerably slower and remains finite even where the detector QPC is already pinched-off in equilibrium. This experimentally observed excess contribution of the normalized  $g_{cf}$  versus  $T_0(E_F)$  signals that the counterflow current carrying electrons are excited above the Fermi level. Converting the shift in  $V_3$  [see the bar in Fig. 3(b)] to energy, we find a characteristic excitation energy of  $E^* \approx 0.5$  meV. This is consistent with a recently reported 1 meV bandwidth excitation provided by the drive QPC for electrons in a nearby double-dot quantum ratchet [14].

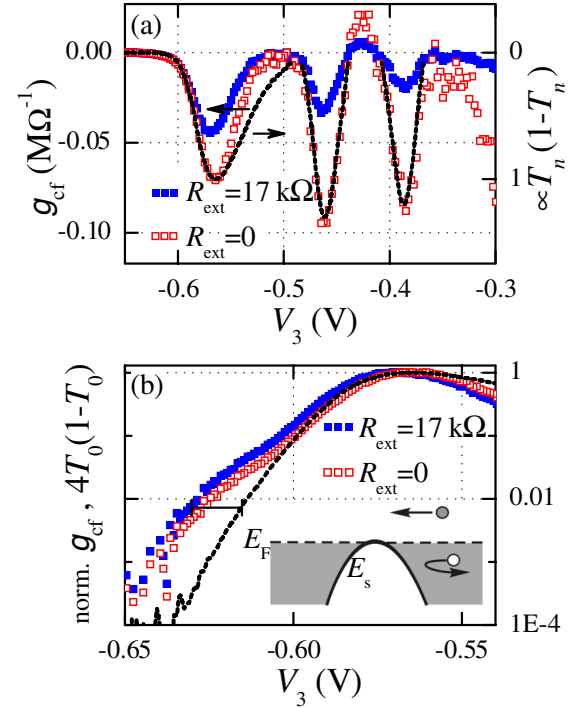


FIG. 3 (color online). (a)  $g_{cf}$  as a function of the detector QPC gate voltage  $V_3$ . Closed symbols correspond to the  $g_{cf}$  measured at a finite external resistance  $R_{ext} = 17$  k $\Omega$ , while open symbols show the corrected counterflow conductance  $R_{ext} = 0$  (see text). Also shown are the transmission functions  $T_n(1 - T_n)$  for the three lowest 1D subbands of the detector QPC (dashed lines), scaled to fit the corrected data. During the  $g_{cf}$  measurement the drive bias is modulated with a 230  $\mu$ V rms signal about the mean value  $V_{drive} = +2.05$  mV. (b) Normalized  $g_{cf}$  [symbols as in (a)] and transmission function of the lowest 1D detector QPC subband  $4T_0(1 - T_0)$  (dashed line) as a function of  $V_3$ . The scale bar shows a gate voltage interval corresponding to a change of the 1D subband energy by 0.5 meV. Inset: Sketch of possible scattering processes of nonequilibrium electrons and holes at a partially transmitting detector QPC.

Next we study the counterflow effect between spatially shifted QPCs. Figure 4 shows  $I_{cf}$  through the nearly pinched-off detector QPC as a function of the bias on the drive QPC, which is formed either with gate 10 or gate 6, while gate 8 is now grounded (Fig. 1). Despite the shift of the drive QPC position relative to the detector QPC by about 300 nm, the odd drive bias dependence of the counterflow current found in Fig. 2 is practically preserved. This indicates that the excitation of electrons in one of the leads of the detector QPC is not restricted to the close vicinity of the drive QPC.

The oscillations of the counterflow conductance  $g_{cf}$  in Fig. 3 are reminiscent of thermopower oscillations that have been investigated on individual QPCs [15,16]. This suggests that  $I_{cf}$  is caused by an energetic imbalance across the detector QPC. If the bottom of the  $n$ th 1D subband of the detector QPC is well separated from the Fermi energy in comparison to the characteristic excitation energy, i.e., if

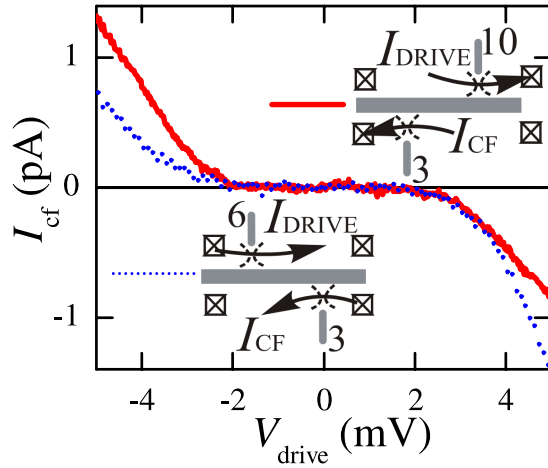


FIG. 4 (color online). Drive bias dependence of the counterflow current through the pinched-off detector QPC for the drive QPC formed with gate 6 (dotted line) or gate 10 (solid line). The detector QPC conductance is about  $G_{\text{det}} = 5 \text{ G}\Omega^{-1}$ . The drive QPCs are tuned to provide the maximal effect. Insets: sketches of the two counterflow measurements. The directions of currents are shown for the case of  $V_{\text{drive}} > 0$ .

$|E_S^n - E_F| \gg E^*$ , this subband is either fully transmitting [ $T_n(E) = 1$ ] or closed ( $T_n(E) = 0$ ). In both cases electrons (holes) excited by  $E^*$  above (below)  $E_F$  are equally transmitted and  $g_{\text{cf}} = 0$ . In contrast, if  $E_S^n \approx E_F$  excited electrons are more likely transmitted than excited holes [see inset of Fig. 3(b)], resulting in  $g_{\text{cf}} \neq 0$ .

The energetic imbalance across the detector QPC we propose to be caused by phonon-based energy transfer from the drive QPC. The excess energy of carriers injected across the drive QPC is mainly relaxed by emission of acoustic phonons. We consider the drive QPC in the nonlinear regime near pinch-off where  $\mu_S - \mu_D \gg \Delta$  and the transmission probability is strongly energy dependent (the source and drain leads are defined so that their chemical potentials satisfy  $\mu_S > \mu_D$ ). In this case electrons injected into the drain lead have an excess energy of about  $e|V_{\text{drive}}| \equiv \mu_S - \mu_D$ , whereas the source lead remains essentially in thermal equilibrium [17]. Hence acoustic phonons are predominantly generated in the drain lead of the drive QPC. Because of this asymmetry, electron-hole pairs are excited preferentially in the adjacent lead of the detector QPC [18]. This gives rise to  $I_{\text{cf}}$  directed opposite to the current through the drive QPC (and  $g_{\text{cf}} < 0$ ). The data in Fig. 2 clearly show that the counterflow effect is only observed in the nonlinear regime of the drive QPC.

For a rough estimate we consider injected electrons with a momentum relaxation time of 60 ps limited by elastic scattering and an energy relaxation time of 1 ns [19,20]. Assuming isotropic phonon emission we estimate an energy transfer ratio which can account for the observed value of  $I_{\text{cf}}/I_{\text{drive}}$  within 1 order of magnitude.

In summary, the current in a strongly biased drive QPC generates a current flowing in the opposite direction through an adjacent unbiased detector QPC. This counterflow current is maximal in between the conductance plateaus of the detector QPC. The effect is most pronounced near pinch-off of the drive QPC, where it behaves strongly nonlinearly. We interpret the results in terms of an asymmetric phonon-based energy transfer.

The authors are grateful to V.T. Dolgoplov, A.W. Holleitner, C. Strunk, F. Wilhelm, I. Favero, A.V. Khaetskii, N.M. Chtchelkatchev, A.A. Shashkin, D.V. Shovkun and P. Hänggi for valuable discussions and to D. Schröer and M. Kroner for technical help. We thank the DFG via No. SFB 631, the BMBF via No. DIP-H.2.1, the Nanosystems Initiative Munich (NIM) and VSK the A. von Humboldt foundation, RFBR, RAS, and the program ‘‘The State Support of Leading Scientific Schools’’ for support.

- [1] V.F. Gantmakher and Y.B. Levinson, *Carrier Scattering in Metals and Semiconductors* (North-Holland, Amsterdam, 1987).
- [2] T.J. Gramila *et al.*, Phys. Rev. Lett. **66**, 1216 (1991).
- [3] T.J. Gramila *et al.*, Phys. Rev. B **47**, 12957 (1993); H. Rubel *et al.*, Semicond. Sci. Technol. **10**, 1229 (1995).
- [4] B. Laikhtman *et al.*, Phys. Rev. B **41**, 9921 (1990).
- [5] X.G. Feng *et al.*, Phys. Rev. Lett. **81**, 3219 (1998).
- [6] J.G.S. Lok *et al.*, Phys. Rev. B **63**, 041305 (2001).
- [7] P. Debray *et al.*, J. Phys. Condens. Matter **13**, 3389 (2001); P. Debray *et al.*, Semicond. Sci. Technol. **17**, R21 (2002).
- [8] M. Yamamoto *et al.*, Science **313**, 204 (2006).
- [9] B.J. van Wees *et al.*, Phys. Rev. Lett. **60**, 848 (1988); D.A. Wharam *et al.*, J. Phys. C **21**, L209 (1988).
- [10] A. Kristensen *et al.*, Phys. Rev. B **62**, 10950 (2000).
- [11] L.I. Glazman and A.V. Khaetskii, JETP Lett. **48**, 591 (1988).
- [12] For increasing  $G_{\text{det}}$ , the noises in the detector circuit increase, making the dc measurements very difficult.
- [13] The input resistance of the  $I$ - $V$  amplifier, the Ohmic contacts, and wiring resistances result in  $R_{\text{ext}} = 17 \text{ k}\Omega$ . The validity of the above formula has been checked by applying an additional  $47 \text{ k}\Omega$  resistor in series to  $R_{\text{ext}}$ .
- [14] V.S. Khrapai *et al.*, Phys. Rev. Lett. **97**, 176803 (2006).
- [15] L.W. Molenkamp *et al.*, Phys. Rev. Lett. **68**, 3765 (1992); H. van Houten *et al.*, Semicond. Sci. Technol. **7**, B215 (1992).
- [16] A.S. Dzurak *et al.*, J. Phys. Condens. Matter **5**, 8055 (1993).
- [17] A. Palevski *et al.*, Phys. Rev. Lett. **62**, 1776 (1989); for asymmetric heating in 3D see U. Gerlach-Meyer and H.J. Queisser Phys. Rev. Lett. **51**, 1904 (1983).
- [18]  $|I_{\text{cf}}|$  is reduced for  $V_{\text{drive}} < 0$  ( $> 0$ ) and the drive QPC shifted to the left-hand (right-hand) side of the detector QPC (Fig. 4). This is understood in terms of absorption of phonons in both leads of the detector QPC.
- [19] B.K. Ridley, Rep. Prog. Phys. **54**, 169 (1991).
- [20] A.A. Verevkin *et al.*, Phys. Rev. B **53**, R7592 (1996).